Water Research 106 (2016) 86–97

Contents lists available at ScienceDirect

Water Research

journal homepage: www.elsevier.com/locate/watres

Biofouling in forward osmosis systems: An experimental and numerical study

Szilárd S. Bucs [a, *], Rodrigo Valladares Linares [a], Johannes S. Vrouwenvelder [a, b, c], Cristian Picioreanu [b]

[a] King Abdullah University of Science and Technology (KAUST), Water Desalination and Reuse Center (WDRC), Division of Biological and Environmental Science and Engineering (BESE), Thuwal 23955-6900, Saudi Arabia
[b] Department of Biotechnology, Faculty of Applied Sciences, Delft University of Technology, Julianalaan 67, 2628 BC Delft, The Netherlands
[c] Wetsus, European Centre of Excellence for Sustainable Water Technology, Oostergoweg 9, 8911 MA Leeuwarden, The Netherlands

ARTICLE INFO

Article history:
Received 21 March 2016
Received in revised form
5 September 2016
Accepted 19 September 2016
Available online 20 September 2016

Keywords:
Forward osmosis fouling
Water filtration
Desalination
Water reuse
Numerical model
Spiral-wound membrane module

ABSTRACT

This study evaluates with numerical simulations supported by experimental data the impact of biofouling on membrane performance in a cross-flow forward osmosis (FO) system. The two-dimensional numerical model couples liquid flow with solute transport in the FO feed and draw channels, in the FO membrane support layer and in the biofilm developed on one or both sides of the membrane. The developed model was tested against experimental measurements at various osmotic pressure differences and in batch operation without and with the presence of biofilm on the membrane active layer. Numerical studies explored the effect of biofilm properties (thickness, hydraulic permeability and porosity), biofilm membrane surface coverage, and biofilm location on salt external concentration polarization and on the permeation flux. The numerical simulations revealed that (i) when biofouling occurs, external concentration polarization became important, (ii) the biofilm hydraulic permeability and membrane surface coverage have the highest impact on water flux, and (iii) the biofilm formed in the draw channel impacts the process performance more than when formed in the feed channel. The proposed mathematical model helps to understand the impact of biofouling in FO membrane systems and to develop possible strategies to reduce and control biofouling.

1. Introduction

Forward osmosis (FO) is a membrane technology in rapid development, based on the difference in osmotic pressure between two liquids separated by a semi-permeable membrane, with a range of possible water treatment applications. Compared to other membrane filtration processes like reverse osmosis or nanofiltration, in FO almost no external hydraulic pressure is required for the process (Mulder, 1996). The driving force in FO is the osmotic pressure difference, such that water is extracted from the low osmotic pressure solution, also referred to as feed water, into the high osmotic pressure draw solution. Forward osmosis (FO) can play a bridging role in the integration of upstream and downstream water treatment processes, and could reduce energy consumption of the entire desalination or water recovery and reuse processes (Valladares Linares et al., 2014b). One of the main advantages of FO compared to conventional membrane processes for desalination and wastewater recovery (i.e. nanofiltration, NF, and reverse osmosis, RO) is the limited amount of external energy required to extract water from the feed solution (Valladares Linares et al., 2014b).

Use of FO for water reclamation was demonstrated in applications like oil/gas wastewater (Hickenbottom et al., 2013), landfill wastewater treatment and water recycling in space missions (Cath et al., 2005; Holloway et al., 2007). Bench scale tests demonstrated the potential of FO in municipal wastewater recovery combined with seawater desalination processes (Valladares Linares et al., 2013; Werner et al., 2013). Other studies evaluated the possibility of using FO systems as a pretreatment in membrane desalination

* Corresponding author. King Abdullah University of Science and Technology (KAUST), Water Desalination and Reuse Center (WDRC), Division of Biological and Environmental Science and Engineering (BESE), Al-Jazri Bldg, Thuwal 23955-6900, Saudi Arabia.
E-mail addresses: Szilard.Bucs@kaust.edu.sa (S.S. Bucs), Rodrigo.Valladares@kaust.edu.sa (R. Valladares Linares), Hans.Vrouwenvelder@wetsus.nl, Johannes.Vrouwenvelder@kaust.edu.sa, J.S.Vrouwenvelder@tudelft.nl (J.S. Vrouwenvelder), C.Picioreanu@tudelft.nl (C. Picioreanu).

http://dx.doi.org/10.1016/j.watres.2016.09.031
0043-1354/

technologies for low-pressure desalination processes while simultaneously recovering water from a recycled feed solution (Achilli et al., 2014; Boo et al., 2013; Hoover et al., 2011). For desalination applications of FO, there are two possible approaches, *direct* and *indirect* desalination. In a *direct* FO desalination processes fresh water is directly extracted from seawater or brackish water by using the high salinity water as feed solution and an osmotic reagent as draw solution. An additional process is required for fresh water recovery from the diluted draw solution (Li et al., 2013; McCutcheon et al., 2005). A full-scale plant commissioned in 2012 is demonstrating the benefits and the viability of *direct* FO desalination (Modern Water Inc, 2012). In *indirect* FO desalination, the high salinity water is used as draw solution and an impaired water such as secondary wastewater effluent is used as of feed solution (Valladares Linares et al., 2013). The attractiveness of *indirect* FO desalination beside the low-cost draw solution (seawater or brackish water) relies on the diluted draw solution which can be used as feed water in a subsequent desalination process like reverse osmosis, thus reducing the cost of the entire desalination process (Yangali-Quintanilla et al., 2011).

However, as in other membrane filtration processes, FO also has the potential of membrane fouling. In certain FO operation conditions, the membrane can suffer from fouling on one side or on both sides. During *indirect* FO desalination when both the feed (secondary wastewater effluent) and the draw (seawater) solutions have fouling potential, deposition of unwanted material on the membrane surface can occur. Similar to other membrane filtration processes (e.g. reverse osmosis), accumulation and growth of microorganisms on the membrane surface is highly possible, leading to biofouling (Shannon et al., 2008; Vrouwenvelder et al., 2008). Only a few studies investigated the impact of biofouling on FO systems (Valladares Linares et al., 2014a; Yoon et al., 2013; Zou et al., 2013). Yoon et al. (2013) showed that the occurrence of biofouling in FO is less severe regarding flux decline when comparing to reverse osmosis. Zou et al. (2013) and Valladares Linares et al. (2014) investigated the impact of different spacer geometries in a cross-flow system on biofouling. Both studies showed an increase in water flux with the spacer inserted in the flow channel. Also noted was that the impact of the same amount of biomass on flux decline was lower when using a thicker spacer (Valladares Linares et al., 2014a). However, none of the FO membrane fouling studies investigated the impact of biofouling on both sides of the membrane simultaneously.

An important particularity of FO membrane filtration compared to other membrane systems such as reverse osmosis and/or ultrafiltration is a different occurrence of concentration polarization (CP). In FO systems three kinds of CP are distinguished: concentrative and dilutive external concentration polarization (ECP) and internal concentration polarization (ICP). The concentrative ECP corresponds to that observed in reverse osmosis systems. Unlike in RO systems, the dilutive ECP occurs in the draw solution side of the membrane due to the permeate flux and ICP takes place in the membrane porous support layer. It was shown that both external concentration polarization effects reduce the process driving force (i.e., the osmotic pressure difference), however their impact on water flux is minor. The most important and process-limiting concentration polarization was found to be the internal concentration polarization (McCutcheon and Elimelech, 2006). Consequently, the difference in driving force and its impact on the filtration processes prevent the direct transplantation of research results from different membrane systems, for example from NF and RO to FO.

The novelty of is work consists in the evaluation of biofouling effects on membrane performance in a cross-flow FO system with numerical simulations, also supported by experimental studies. The numerical model was used to study the impact of (i) biofilm properties (thickness, hydraulic permeability, and porosity), biofilm membrane surface coverage, and biofilm location (feed channel, draw channel and both) on FO membrane performance, and (ii) biofouling on external concentration polarization in different FO operation conditions.

2. Materials and methods

2.1. Experimental setup

A lab-scale FO membrane system was used for the experimental evaluation of permeation fluxes without and with biofilm development on the membranes. Two peristaltic pumps (Cole-Parmer) circulated in closed loop the feed and draw solutions at similar cross-flow velocities (8.6 cm s^{-1}). The pumps were connected to two reservoirs with the same volume (1.25 L), one for the feed solution and one for the draw solution. Each reservoir was placed on a digital scale (Mettler Toledo) connected to a computer. The water flux through the membrane was calculated from the change in weight of the reservoirs. All experiments were performed at 20 °C.

Cellulose triacetate (HTI, Scottsdale, AZ) forward osmosis membrane with a thickness of ~50 μm was used for the experiments. In all cases, the membrane active layer faced the feed solution while the support layer was in contact with the draw solution. This configuration was shown to be the most effective to prevent membrane fouling (Mi and Elimelech, 2008; Wang et al., 2010).

The membrane was placed into a custom-made flow cell from poly (methyl methacrylate) (PMMA), with an active membrane area of 20 cm^2. The flow cell was designed to allow operation without and with the presence of spacer in the feed and draw channels. The feed and draw channels height were the same and could fit 46 mil (1168 mm) thick spacers. For the studies with spacer, a 46 mil spacer produced by Hydration Technology Innovation (HTI, Scottsdale, AZ) was used on both sides of the membrane. A more detailed description of the flow cell can be found in previous studies (Li et al., 2012).

For flux measurements at various osmotic pressure differences sodium chloride (NaCl) solutions were prepared. The feed solution salt concentration was kept constant at 0.58 kg m^{-3} while the draw solution concentration was varied from 5.8 kg m^{-3} to 78.8 kg m^{-3}.

The biofouling experiments were run in a repeated batch mode. Each batch cycle was interrupted after 20 h of operation and the feed and draw solutions were replaced by fresh solutions (salt concentrations of 2 kg m^{-3} in feed and 40 kg m^{-3} in draw), then the next cycle was started. To ensure biofilm formation in the feed channel, a municipal secondary effluent (Al-Ruwais wastewater treatment plant, Saudi Arabia) was used as feed solution for the first 20 h. The effluent characteristics were: chemical oxygen demand (COD) 25 mg L^{-1}, total organic carbon (TOC) 4.84 mg L^{-1}, pH 7.1, conductivity 2.33 mS cm^{-1}, osmotic pressure 0.38 bar, total suspended solids (TSS) 2.25 mg L^{-1} and volatile suspended solids (VSS) 2.15 mg L^{-1}. The adenosine triphosphate (ATP) concentration of the effluent was 215 pg mL^{-1}, which corresponds to a bacterial cell concentration of approx. 10^7 cells·mL^{-1}. For the subsequent five FO filtration cycles, the feed solution was a synthetic municipal wastewater as described in (Valladares Linares et al., 2014a, 2013), initially with 360 mg COD·L^{-1}, 115 mg TOC·L^{-1} and pH 5.66. All the chemicals were purchased from Sigma-Aldrich (Munich, Germany) and had a purity grade higher than 99.5%. All solutions were prepared with deionized (DI) ultra-pure water (Valladares Linares et al., 2014a, 2013).

2.2. Model description

A two-dimensional mathematical model was developed to investigate numerically the impact of biofouling on the performance of forward osmosis processes. The model includes liquid flow coupled with the mass transport of the solute (salt) through the feed and draw channels, through the asymmetric permeable membrane, and through a biofilm present on the FO membrane.

2.2.1. Model geometry

Without biofilm, the model geometry included three domains: feed and draw channels separated by a membrane support layer (Fig. 1a), while the thin membrane active layer was assimilated with a boundary in this model. The flow channel length (L_X) was chosen tenfold smaller than the length of the flow cell used for the experimental studies. This length was small enough to allow performing computationally efficient numerical simulations, while maintaining a size representative for the FO system (i.e., including several spacer fibers). The heights of the two flow channels (L_Y) and membrane support layer thickness (L_S) were those used in the experimental studies. When the biofilm was present, it constituted a fourth planar domain with thickness L_B. Although not completely realistic, the feed and draw channel spacer fibers were circular and arranged in a zig-zag configuration mimicking a two-dimensional axial slice in a three-dimensional flow channel (Fig. 1b). The diameter (d_M) and distance between the spacer fibers (L_M) corresponded with the 46 mil spacer geometry used for the experimental studies (Table 1).

2.2.2. Fluid flow

The flow in the feed and draw channels was calculated from steady-state laminar Navier-Stokes equations (eq. (1)):

$$\begin{aligned} \rho(\mathbf{u}\cdot\nabla)\mathbf{u} + \nabla p &= \nabla\cdot(\eta\nabla\mathbf{u}) \\ \nabla\cdot\mathbf{u} &= 0 \end{aligned} \tag{1}$$

where $\mathbf{u} = (u_x, u_y)$ is the vector of local liquid velocity, p is the pressure, ρ and η are the density and dynamic viscosity of the solution at 293 K, respectively. The steady-state laminar flow assumption is justified considering the low Re number used in the experiments (Re ≈ 80, calculated according to Schock and Miquel, 1987), as shown in Bucs et al. (2015).

The membrane support layer and biofilm domains were treated as porous media and Brinkman flow was assumed according to eq. (2):

$$\begin{aligned} \frac{\eta}{K}\mathbf{u} + \nabla p &= \frac{\eta}{\varepsilon}\nabla^2\mathbf{u} \\ \nabla\cdot\mathbf{u} &= 0 \end{aligned} \tag{2}$$

where K and ε are the permeability and porosity of membrane support layer (K_{WS} and ε_S) and biofilm (K_B and ε_B).

The boundary conditions used are listed in Table 2. Fully developed laminar flow profiles with average velocity u_{in} were imposed at the feed and draw channel inlets, while the pressure was set to zero at the outlet boundaries. No-slip conditions were applied to the spacer surface and to the bottom and top boundaries of the feed and draw channels, respectively. Flow continuity was assumed between the support layer or biofilm surface and the draw or feed channels. A flux of water J_W was imposed on the membrane active layer, proportional with the local osmotic pressure difference ($\Delta\pi$) and the permeability for water (A) (eq. (3) (Sagiv et al., 2014):

$$J_W = A\left(\pi_{draw} - \pi_{feed}\right) = A\cdot\Delta\pi \tag{3}$$

The osmotic pressures in the draw and feed solution (π_{draw} and π_{feed}) were calculated from Van't Hoff eq. (4) (Mulder, 1996, p. 283):

$$\pi = 2C\cdot R\cdot T \tag{4}$$

function of local salt concentrations C_{draw} and C_{feed} at the membrane surface, universal gas constant R and temperature T (Table 2).

2.2.3. Salt transport

Sodium chloride was assumed the only soluble compound relevant for this model, transported by convection and diffusion in both of the flow channels (eq. (5)).

$$D\nabla^2 C - \mathbf{u}\nabla C = 0 \tag{5}$$

where D is the diffusion coefficient and C is the local salt concentration. The salt diffusion coefficient was considered equal in the feed and draw solutions (D_W), whereas lower values were taken in the membrane support layer (D_S) and in the biofilm (D_B) domains (Table 1).

In the inlet, the solutions contained salt with concentrations C_F (feed channel) and C_D (draw channel). Typical no-diffusion conditions applied at the outlet boundaries for both channels, while the spacer surface, bottom and top boundaries were impermeable walls. In FO processes, draw solute leaks through the membrane into the feed side, as described by (Eq. (6), (Sagiv et al., 2014):

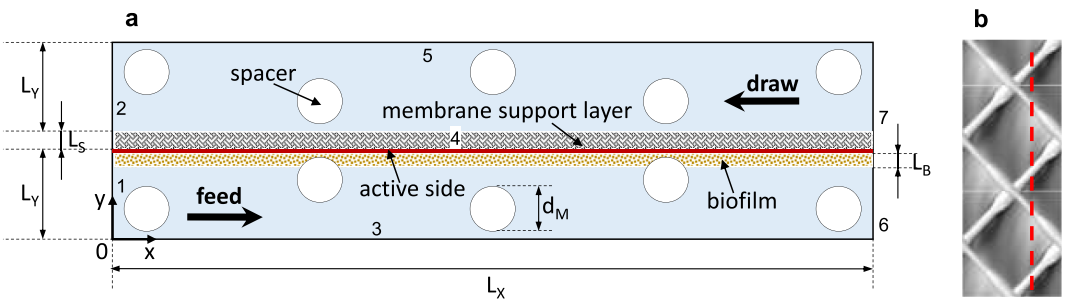

Fig. 1. (a) Illustration of the forward osmosis (FO) model geometry. The model space is divided to three domains: feed and draw channels (blue color, with bold arrows indicating the flow directions) and membrane support layer (woven grey). The membrane active layer (red line) is facing the feed channel side and it represents a boundary. When present, the biofilm (yellow dotted zone) constitutes a fourth domain. The geometry dimensions are explained in Table 1. Numbers represent the different boundaries of the computational domains, as explained in Table 2. (b) Spacer fibers are arranged in such a way to mimic an imaginary 2D plane along the red dashed line in a 3D flow channel. (For interpretation of the references to colour in this figure legend, the reader is referred to the web version of this article.)

Table 1
Model parameters and experimental conditions.

Parameter	Symbol	Value	Unit	Source
Model geometry				
channel length	L_X	10	mm	chosen
channel height	L_Y	1.17	mm	46 mil Filmtech™ spacer
membrane thickness	L_S	50	μm	Valladares Linares et al., 2014
spacer fiber thickness	d_M	0.58	mm	Valladares Linares et al., 2014
spacer mesh size	L_M	4.1	mm	Valladares Linares et al., 2014
Experimental conditions				
average inlet flow velocity	u_{in}	8.6	Cm s^{-1}	Valladares Linares et al., 2014
feed salt concentration inlet or initial (biofouling case)	$C_{F,0}$	2	kg m^{-3}	Valladares Linares et al., 2014
draw salt concentration inlet or initial (biofouling case)	$C_{D,0}$	40	kg m^{-3}	Valladares Linares et al., 2014
initial solution volume in feed reservoir	$V_{F,0}$	1.25	L	Valladares Linares et al., 2014
initial solution volume in draw reservoir	$V_{D,0}$	1.25	L	Valladares Linares et al., 2014
membrane area	A_M	20	Cm^2	Valladares Linares et al., 2014
temperature	T	293	K	Valladares Linares et al., 2014
Water and solute properties				
feed water density	ρ_F	999	kg m^{-3}	Crittenden et al., 2012
draw solution density	ρ_D	1020	kg m^{-3}	McCutcheon and Elimelech, 2006
water viscosity	η	10^{-3}	Pa s	Crittenden et al., 2012
salt diffusion coefficient in water	D_W	1.33×10^{-9}	m^2 s^{-1}	McCutcheon and Elimelech, 2006
salt diffusion coefficient in support layer	D_S	0.18×10^{-9}	m^2 s^{-1}	Calculated as L_S/K_S
Membrane properties				
water permeability	A	0.57	L m^{-2} h^{-1} bar	Phillip et al., 2010
solute permeability	B	0.33	L m^{-2} h^{-1}	Phillip et al., 2010
membrane structural parameter	S	360	μm	McCutcheon and Elimelech, 2006
salt resistivity of support layer	K_S	2.7×10^5	s m^{-1}	McCutcheon and Elimelech, 2006
water permeability of support layer	K_{WS}	2×10^{-15}	M^2	Dreszer et al., 2013
support layer porosity	ε_S	0.3	–	Calculated as $\tau \cdot L_S/S$(chosen tortuosity $\tau = 2$)
Biofilm properties				
Porosity	ε_B	0.5	–	Radu et al., 2010
Permeability	K_B	10^{-17}	M^2	Dreszer et al., 2013
salt diffusion coefficient in biofilm	D_B	0.66×10^{-9}	m^2 s^{-1}	Calculated as $\varepsilon_B \cdot D_W$
biomass specific growth rate	μ	0.81	d^{-1}	fitted with 46 mil experimental data from Valladares Linares et al., 2014
initial biofilm thickness	$L_{B,0}$	5	μm	Chosen
maximum biofilm thickness	$L_{B,E}$	150	μm	Valladares Linares et al., 2014
biofilm thickness	L_B	150	μm	Valladares Linares et al., 2014

Table 2
Boundary conditions for the FO model geometry presented in Fig. 1a.

Boundary no.	Feed side		Draw side	
	Fluid flow	Salt transport	Fluid flow	Salt transport
1	$u_x = 6u_{in}(1-y/L_y)y/L_y$ $u_y = 0$	$C = C_F$	–	–
2	–	–	$p = 0$	$-\mathrm{n}\cdot D_W\nabla C = 0$
3 and spacer	$\mathbf{u} = 0$	$-\mathrm{n}\cdot D_W\nabla C = 0$	–	–
4	$u_x = 0$ $u_y = -J_W$	$-\mathrm{n}\cdot\mathbf{J} = J_S$	$u_x = 0$ $u_y = J_W$	$-\mathrm{n}\cdot\mathbf{J} = -J_S$
5 and spacer	–	–	$\mathbf{u} = 0$	$-\mathrm{n}\cdot D_W\nabla C = 0$
6	$p = 0$	$-\mathrm{n}\cdot D_W\nabla C = 0$	–	–
7	–	–	$u_x = -6\ u_{in}(1-y/L_y)y/L_y$ $u_y = 0$	$C = C_D$

$$J_S = B\left(C_{draw} - C_{feed}\right) \tag{6}$$

where B is the membrane permeability for salt, and C_{draw} and C_{feed} are the local salt concentrations in the draw and feed channels, respectively. The flux of salt is in opposite direction to the water flux.

2.2.4. Biofilm development

To study the impact of biofilms formed on the membrane on the FO process performance, three cases were investigated: (i) a continuous planar biofilm with thickness increasing in time (thus roughly simulating biofilm growth); (ii) a continuous planar layer with thickness constant in time; and (iii) a patchy biofilm formed by microbial colonies of various size, but constant in time. In the first two cases, the biofilm of uniform thickness covered the whole membrane area, while in the third case the patchy biofilm covered only 50% of the membrane, but had the same biofilm volume as in the second case. By assuming, for simplicity, unlimited biomass growth at constant specific rate μ and constant biomass concentration in the biofilm, the increase in biofilm thickness L_B in case (i) is represented by eq. (7):

$$L_B = L_{B0}\exp(\mu t) \tag{7}$$

In all cases, the biofilm was represented as a computational domain and flow continuity was applied at the moving biofilm-liquid interface (Fig. 1).

Water and solute transport in biofilms are functions of the biofilm properties and morphology. According to Darcy's law, permeation flux through the biofilm, J_W, is function of the pressure

drop over the biofilm, fluid viscosity, biofilm permeability and thickness (eq. (8)) (Dreszer et al., 2013):

$$J_W = \frac{K_B}{\eta \cdot L_B} \Delta p \tag{8}$$

This means that also the hydraulic resistance, R_B defined by eq. (9), is time dependent because the biofilm thickness can change in time:

$$R_B = \frac{L_B}{K_B} \tag{9}$$

2.2.5. Model solution

The two-dimensional liquid flow and salt transport were solved in COMSOL Multiphysics (v5.1, Comsol Inc., Burlington, MA), on a triangular finite-element mesh with a maximum size of 5 μm, using a stationary solver. In case of biofilm growth, a moving mesh procedure was applied for the time-dependent biofilm-liquid interface, while the liquid flow and salt transport were also solved in time.

2.2.6. Simulation of batch operation

To simulate the batch process, the model was extended to include the feed solution concentration and draw solution dilution in time, together with the change in feed and draw solution volumes, V_F and V_D (eqs.(10)–(13)):

$$\frac{dV_F}{dt} = -J_W \cdot A_M; \tag{10}$$

$$\frac{dC_F}{dt} = (J_W C_F + J_S) \cdot \frac{A_M}{V_F} \tag{11}$$

$$\frac{dV_D}{dt} = J_W \cdot A_M; \tag{12}$$

$$\frac{dC_D}{dt} = -(J_W C_D + J_S) \cdot \frac{A_M}{V_D} \tag{13}$$

where C_F and C_D are the salt concentrations of feed and draw solutions, and A_M is the membrane area. The initial values are listed in Table 1.

3. Results and discussion

The aim of this study was to evaluate the impact of biofilms on the performance of FO processes. Although concentration polarization is considered in the developed model, a detailed study of its impact on process performance here is out of scope. First, a two-dimensional model was developed for the FO without biofilm presence and the results were compared with experimental data at different osmotic pressures and in a batch operation. Second, the model was extended to include biofilm development in the feed channel and compared with experimental results. Third, the calibrated model was used to investigate the biofilm impact on concentration polarization, and the effects of biofilm properties (i.e. thickness, roughness, porosity, and permeability) on the performance of an FO process. Finally, the influence of biofilm location (i.e., in draw channel, in feed channel or in both) was evaluated.

3.1. Evaluation of the forward osmosis model

To evaluate the proposed numerical model, simulations were compared with experimental measurements. In total three sets of flux measurements were performed: (i) at different osmotic pressures, (ii) in batch operation to record the flux decline due to solution dilution in time and (iii) with biofilm growth under batch operation.

3.1.1. Water flux increase with increasing osmotic pressure

Water flux was experimentally measured at various salt concentrations in the feed and draw solutions. For these experimental measurements, no spacer was used in the flow cell and the conditions were set to minimize the possibility of biofilm formation. Consequently, no spacer and no biofilm were considered in this model version. The feed solution salt concentration (NaCl) was kept at 0.58 kg m^{-3} for all the experimental measurements and the concentration in the draw solution was varied from 5.8 kg m^{-3} up to 78.8 kg m^{-3} in steps of 14.6 kg m^{-3}. The experimental setup was operated in batch mode, 1 h for each salt concentration, and the average flux in that hour was calculated.

Membrane parameters for the numerical simulations, such as, membrane water permeability ($A = 0.44$ L m^{-2} h^{-1} bar), membrane solute permeability ($B = 0.26$ L m^{-2} h^{-1}) were taken from Phillip et al., 2010. The salt diffusion coefficient in the support layer (D_S), support layer water, and solute permeability (K_{WS}, K_S), were also taken from literature (Dreszer et al., 2013; McCutcheon and Elimelech, 2006) (Table 1). To evaluate the model and the applied parameters, the flux was calculated at the same solute concentrations in the feed and draw solutions as used in the experiments. Comparing the calculated and measured flux increase with increasing osmotic pressure confirmed that, in this case, the model describes the process accurately without further parameter fitting (Fig. 2).

3.1.2. Flux decline in batch experiments

In a batch FO process, the water flux decreases in time because the draw solution gets diluted, while the feed solution becomes more concentrated in salt. To further test the model in dynamic conditions, the flux decline in a batch process was first experimentally measured. The batch experiment was performed by

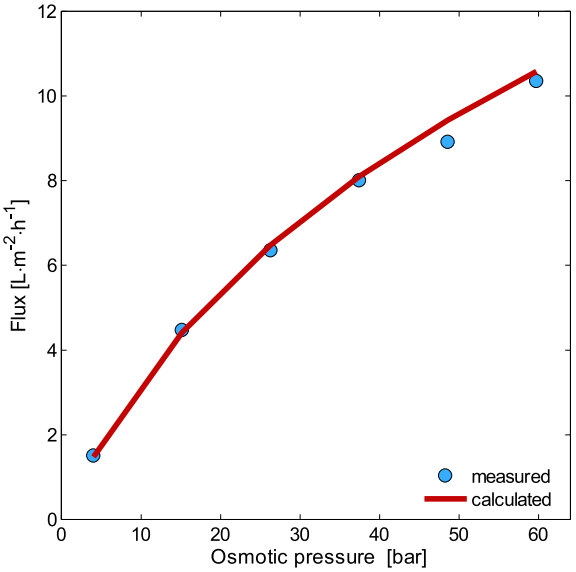

Fig. 2. Experimentally measured (blue circles) and calculated with the developed numerical model (red line) water flux at different osmotic pressure differences, without the presence of spacer or biofilms. Model parameters are presented in Table 1. (For interpretation of the references to colour in this figure legend, the reader is referred to the web version of this article.)

recirculating 1.25 L of feed and draw solutions through the flow channels with spacers for a period of 1200 min (20 h).

For the whole batch period, the model predicts a linear flux decline similar to the experimental results (Fig. 3a). As described by the model eqs. (8)–(11), the flux decline depends on the experimental conditions and membrane properties. For these studies, the 20 cm^2 membrane coupons were cut out from a larger sheet membrane, showing differences in permeability. For FO membranes, a relatively high standard deviation (>30%) in membrane properties is possible, as shown by Phillip et al. (2010). While the experimental conditions were set, the values for membrane properties in the numerical model had to be adjusted to describe the measurements (values from Table 1). In this way, membrane water permeability and the membrane solute permeability were increased by 30 percent in the numerical model compared with the values used in the previous osmotic pressure simulations. By increasing the membrane water permeability, *A*, not only that a higher flux is achieved, but the draw solution is also diluted faster, which results in a more rapid flux decline (Fig. 3a). Higher membrane solute permeability, *B*, also increases the dilution rate of the draw solution, but we found that the water flux decline is more sensitive to the membrane water permeability.

These results were further used to provide consistent initial values and calibrated membrane parameter values for the FO simulations with biofilm.

3.1.3. Flux decline in repeated batch studies with biofilm formation

Repeated batch experiments were performed under conditions favorable for biofilm development in the feed channel (with spacers). For the draw channel, conditions were kept to avoid biofilm development (i.e., no inoculation and no substrate). Flux through the membrane, as a performance parameter for the FO process, was monitored during the experimental period. In each cycle, the water flux declined not only because of dilution of the draw solution but also due to biofilm formation. After each cycle (1200 min) the solutions were replaced by fresh solutions, but the biofilm built up in each cycle remained and increasingly affected the flux (Fig. 3b). As the biomass accumulated in the system, the rate of the flux decline within one cycle increased (i.e. steeper flux-time slopes). The faster water flux decline for the later cycles can be explained by the increased resistance of the developed biofilm (Valladares Linares et al., 2015).

Biofilm properties (such as thickness, permeability, porosity and growth rate) may vary as the biofilm develops. Simulations of the repeated batch experiment were run with simple exponential biofilm growth in the feed channel. This ideal scenario for biofilm growth is probably not realistic for long-term biofilm development, but it proves to be representative for the initial phase of biofilm formation when the nutrients are still in excess (Vrouwenvelder et al., 2009). In the numerical model the biomass growth rate (μ) and the initial biofilm thickness ($L_{B,0}$) were set such that the maximum biofilm thickness ($L_{B,E}$) reached at the end of the five cycles was 150 μm, similarly to the thickness measured by Valladares Linares et al. (2014). To keep the model simple the biofilm porosity (ε_B) was kept constant, while the water permeability of the biofilm (K_B) had to be decreased with the biofilm age. However, for a real biofilm these parameters (thickness, porosity and water permeability) are changing simultaneously with the biofilm age. For the first two cycles, $K_B = 10^{-16}$ m^2, while for last three cycles a smaller value of 10^{-17} m^2 was used in the model to represent the flux measurements (Dreszer et al., 2013; Martin et al., 2014).

In these conditions, the comparison of measured flux decline with the model results shows that the model can describe well the impact of biofilms on the FO process performance (Fig. 3b).

3.2. Biofilm effect on FO performance

The biofilm impact on concentration polarization and the effects of biofilm properties and biofilm location on the performance of an FO process were further evaluated with the calibrated model only, no experimental studies were performed.

3.2.1. Impact of biofilm on water flux and concentration polarization

The effect of spacer presence on water flux was first investigated in a clean FO system. With spacers on both sides of the membrane, a small flux variation was observed along the membrane (±0.15 L m^{-2} h^{-1}), while without spacer the flux increased continuously towards the end of the flow channel because of the

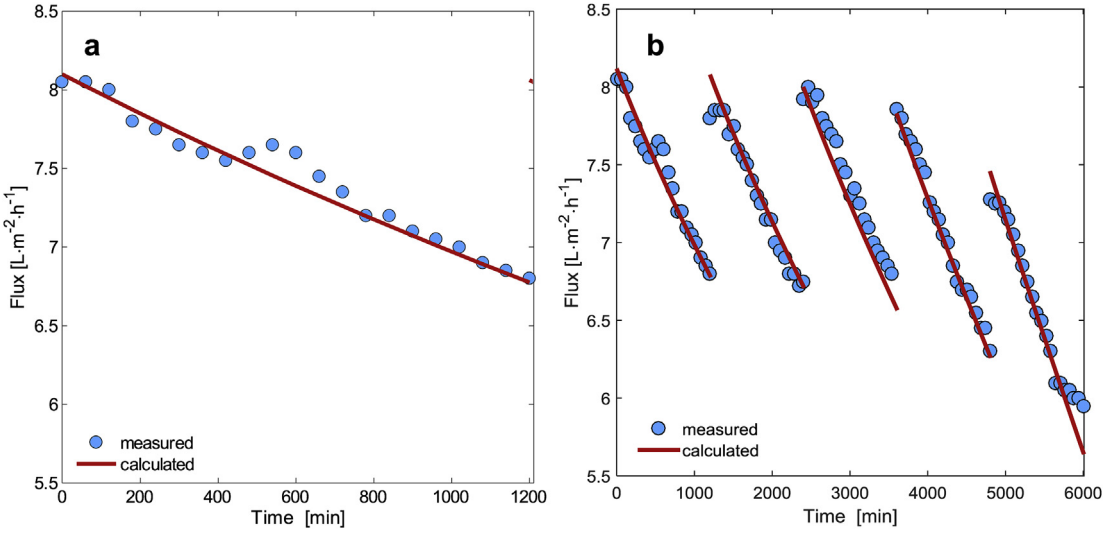

Fig. 3. (a) Measured (blue circles) and calculated (red line) water flux decline over time due to the dilution of draw solution in batch operation, with spacers but without biofilms. (b) Combined impact of dilution and biofilm formation on flux in forward osmosis system operated in repeated batch mode, measured (blue circles) and model (red lines). (For interpretation of the references to colour in this figure legend, the reader is referred to the web version of this article.)

counter flow operation (Fig. 4a, blue lines). The average water flux was only one percent higher with spacer than without. Visualization of the 2-D solute concentration distribution confirms that the presence of spacer has a small influence on the concentration polarization: the maximum solute concentration at the membrane was 2.35 kg m^{-3} (in isolated spots only) compared with an inlet concentration of 2 kg m^{-3} (Fig. 4b). The role of the spacers is to keep the membrane sheets apart and, by enhancing fluid mixing, to reduce concentration polarization at the membrane surface. While in reverse osmosis feed spacers are needed to reduce concentration polarization close to the membrane surface (Radu et al., 2010; Subramani et al., 2006), it is known that in FO processes the concentration polarization at the membrane surface (external concentration polarization, ECP) does not significantly affect the water flux (Qin et al., 2010; Tan and Ng, 2008).

The water flux limiting factor in FO processes is the internal concentration polarization (ICP) within the membrane support layer (Gray et al., 2006; McCutcheon and Elimelech, 2006). However, the water flux considerably decreased (~20 percent) when a continuous biofilm on the feed side of the membrane was included in the model. Although the water flux profile along the membrane is similar to the flux profile without biofilm, a sharp flux decrease at the spacer fibers close to the membrane was observed (Fig. 4a, dashed red line). The sharp flux decrease, corresponding to high ECP, is the result of the 150 μm (L_B) thick biofilm that completely fills up the space between the membrane and spacer fibers close to the membrane (Fig. 4c).

As shown in Fig. 5, the presence of spacer and the ECP became important in the presence of biofilms. The osmotic pressure difference (the driving force of the FO process) decreased with 18 percent (an effective $\Delta\pi = 11.7$ bar, compared with 14.3 bar) in the case when the spacer fibers are far from the membrane (Fig. 5a) and with 50 percent (an effective $\Delta\pi = 7.2$ bar, compared with 14.2 bar) when the fibers are close to the membrane and, thus, in contact with the biofilm (Fig. 5b). The biofilm leads to increased ECP because it drastically limits the convective transport and creates a diffusion-dominated mass transfer layer. This is also reflected in the almost linear concentration profiles in the biofilm and support layer (Fig. 5). At higher water fluxes, the increased contribution of convection may lead to nonlinear concentration profiles in the

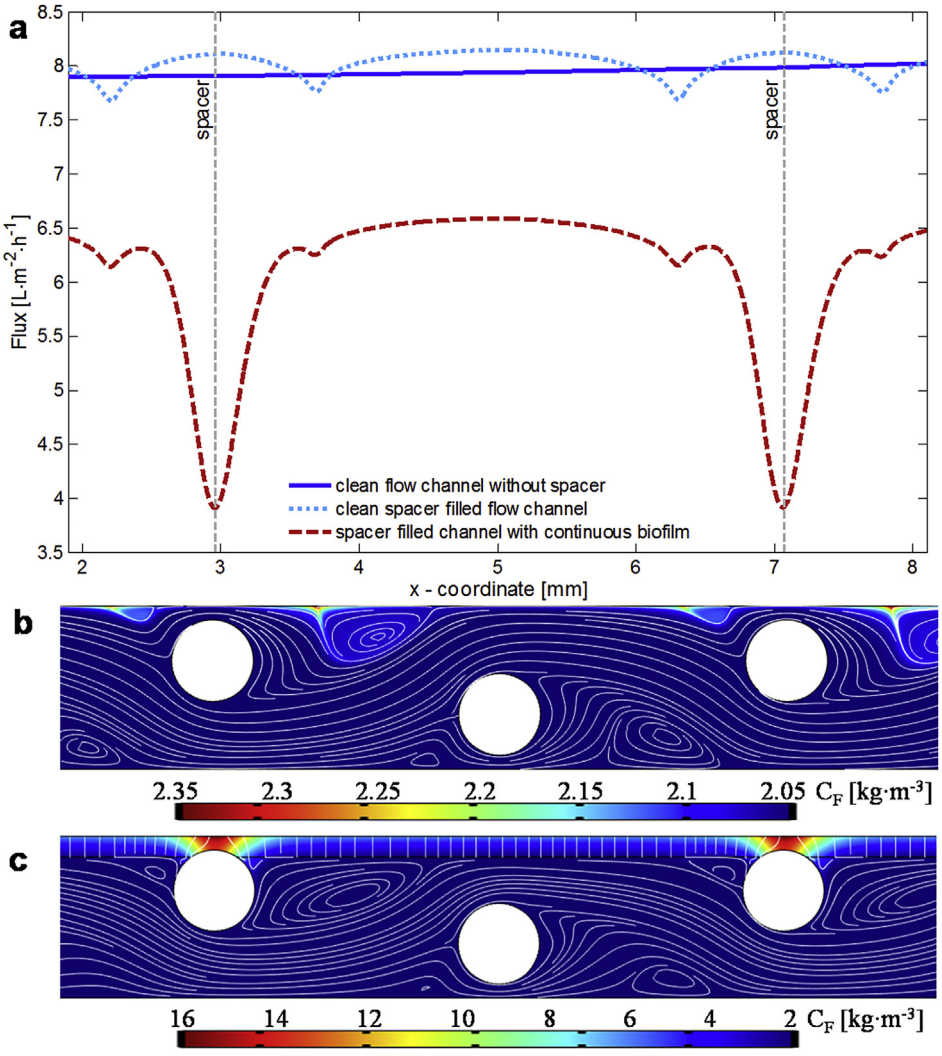

Fig. 4. (a) Calculated water flux along the membrane: without spacer (continuous blue line), with spacer (dotted blue line) and with spacer and biofilm (dashed red line). The vertical dashed grey lines indicate the locations of the spacer fibers close to the membrane surface. (b) Salt concentration field in clean feed channel. (c) Salt concentration field with uniform thickness biofilm on the feed side of the membrane (top figure). The colors in (b) and (c) represent the solute concentration, the white streamlines indicate the water flow (from left to right). The biofilm leads to large concentration polarization and sharp water flux decrease close to the spacer fibers. (For interpretation of the references to colour in this figure legend, the reader is referred to the web version of this article.)

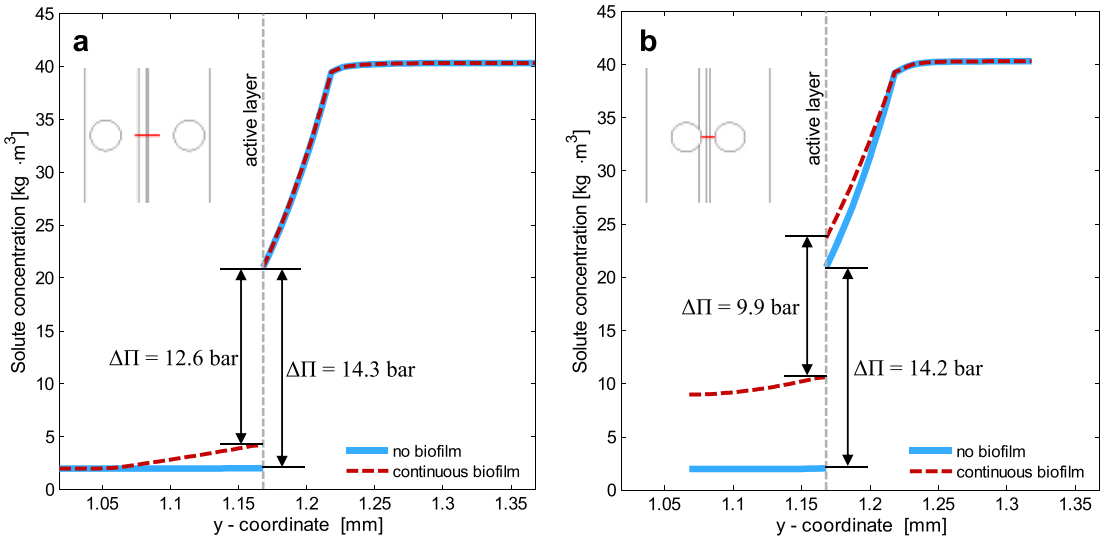

Fig. 5. Calculated salt concentration profiles in the feed channel, membrane support layer and draw channel next to the membrane, without (continuous blue line) and with (dashed red line) a continuous and uniform biofilm layer. (a) Profiles at a location where the spacer fibers are far from the membrane. (b) Profiles at a position where the spacer fibers are close to the membrane. When the biofilm joins the spacer fibers with the membrane (b), the external concentration polarization is highly increased. (For interpretation of the references to colour in this figure legend, the reader is referred to the web version of this article.)

support layer, as reported in earlier studies (Su and Chung, 2011; Suh and Lee, 2013).

In the lab-scale as well as in a full-scale FO system the spacer is in full contact with the membrane surface at several locations. In these locations, the membrane is "shaded", and no water permeation is possible. Areas next to the spacer fibers close to the membrane are favorable locations for biofilm formation (Araújo et al., 2012; Baker et al., 1995; Vrouwenvelder et al., 2009). Furthermore, ECP increases in the biofilm presence and, in the case of a thick and dense biofilm, may even become the limiting factor for the water flux. Similar effects were reported for reverse osmosis systems (Chong et al., 2008; Radu et al., 2010).

3.2.2. *Effect of biofilm properties*

As the biofilm develops on the membrane surface, it becomes part of the separation process. Water and solute transport in biofilms are functions of the biofilm hydraulic permeability K_B and porosity ε_B.

To simulate the impact of biofilms on the FO processes performance, several biofilm parameters had to be defined. However, experimentally measured biofilm hydraulic resistance or permeability values are scarce in the literature (Dreszer et al., 2013; Martin et al., 2014; McDonogh et al., 1994). The reported values for biofilm hydraulic permeability vary between $10^{-15} - 10^{-18}$ m^2 and most of these were measured for biofilms developed in reverse osmosis or microfiltration systems. To evaluate how the hydraulic permeability influences the permeate production in an FO process, parametric sensitivity simulations were performed with increasing biofilm thickness at various biofilm hydraulic permeability (Fig. 6a).

Results showed significant flux decline even for a relatively thin biofilm ($L_B = 5$ μm) when the biofilm hydraulic permeability was $K_B = 10^{-18}$ m^2 (Fig. 6a, continuous red line). However, a compact biofilm with such a low permeability is unlikely to form in FO

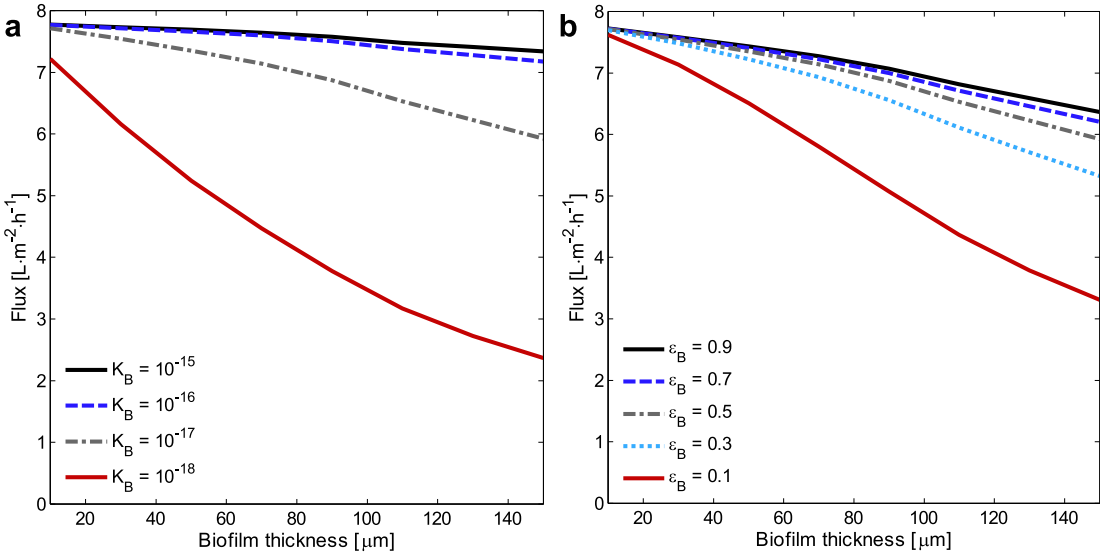

Fig. 6. Calculated flux decline at different biofilm thickness on the membrane feed side, with spacers in the flow channels. (a) Effect of different biofilm permeability (K_B, in m2). (b) Effect of different biofilm porosities (ε_B).

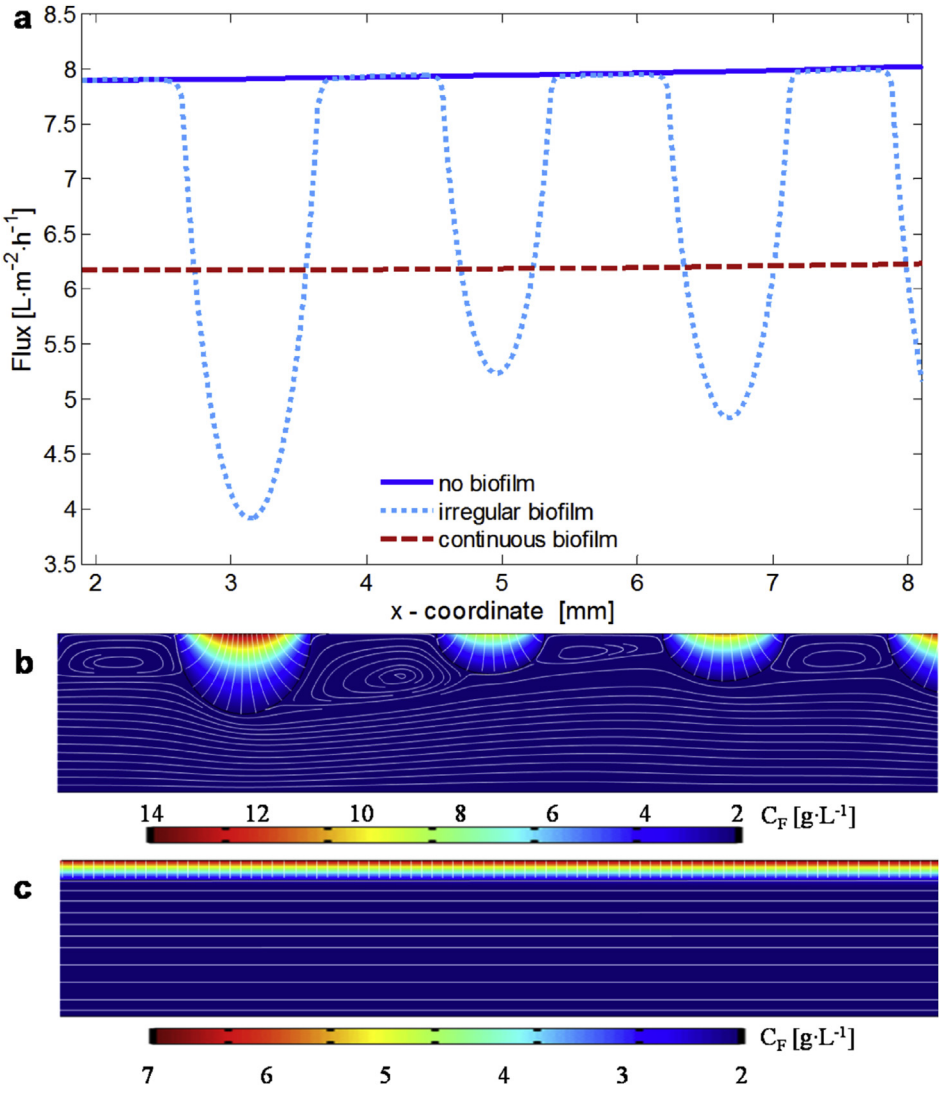

Fig. 7. (a) Calculated water flux along the membrane: without biofilms (continuous blue line), with patchy biofilm (dotted blue line) and with continuous uniform biofilm (dashed red line), on the membrane active side. The average water flux obtained was: 7.9 L $m^{-2}\cdot h^{-1}$ (no biofilm), 6.4 L $m^{-2}\cdot h^{-1}$ (patchy biofilm) and 6 L $m^{-2}\cdot h^{-1}$ (continuous biofilm). (b) Salt concentration field in the patchy biofilm case. (c) Salt concentration field with uniform thickness biofilm. The colors represent the solute concentration, the white streamlines indicate the water flow (from left to right). (For interpretation of the references to colour in this figure legend, the reader is referred to the web version of this article.)

systems due to the relatively low water flux and pressure. On the other hand, high hydraulic permeability values such as 10^{-15} and 10^{-16} m^2 had an insignificant impact on flux even with thick (>100 μm) biofilms. Therefore, for the simulations with biofilm development compared with the experimental data, previously presented, the K_B was set to 10^{-16} m^2 for thin biofilm (first two cycles) and changed to 10^{-17} m^2 as the biofilm got thicker. For the rest of the simulations, the hydraulic permeability was kept constant at 10^{-17} m^2, in line with values reported by Martin et al. (2014).

Beside hydraulic permeability, the biofilm porosity also affects the permeation flux. Porosity can be defined as the volume fraction of the water phase in the biofilm. In general, as a result of spatial distributions of microbial species, biotic and abiotic components, porosity (along with other biofilm parameters) changes with biofilm age and thickness (Zhang and Bishop, 1994). The impact on flux of different biofilm porosities was evaluated (Fig. 6b). Limited information can be found in the literature about biofilm porosity, with values generally varying from 0.2 to 0.9 (Lewandowski, 2000; Picioreanu et al., 2009; Radu et al., 2010; Zhang and Bishop, 1994). Simulations with various porosity and biofilm thickness showed that porosity significantly affects the flux only below values of 0.5, which are usually obtained under fast flow conditions with high erosion and detachment rates. In addition, biofilm maturation can also lead to dense cell layers especially in the deeper part of the biofilm, by this decreasing the biofilm porosity. Moreover, another effect of biofilm porosity is related to the decrease of effective salt diffusion coefficient with decreasing porosity, which leads to enhanced concentration polarization and thus less water flux.

The aim of these simulations was to understand how each parameter individually affects the water flux. Nevertheless, all three biofilm parameters (permeability, porosity and thickness) are linked and, in real biofilm systems, all change simultaneously in time. It was shown that in FO (where no applied hydraulic pressure is present) the biofilms tend to grow thicker and more porous and patchy, therefore with less hydraulic resistance (Kwan et al., 2015). This is contrary to what was observed for biofilms formed under applied hydraulic pressure in RO systems (Kwan et al., 2015; Xie et al., 2015). Clearly, measurements obtained in FO conditions are needed to reveal how the biofilm parameters change in time and to

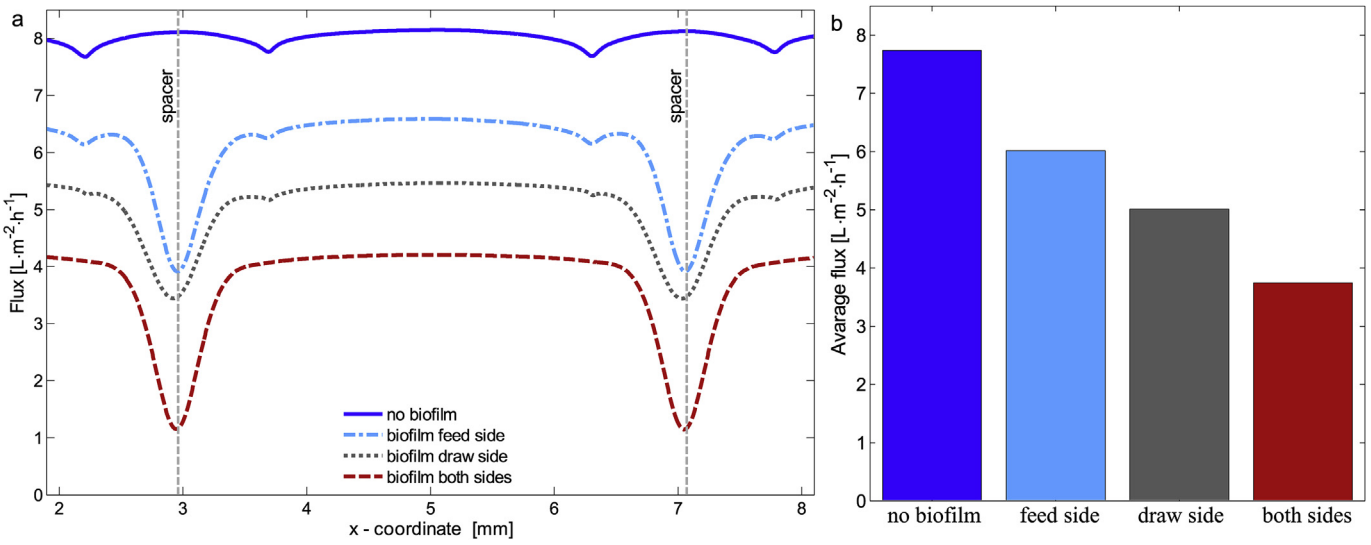

Fig. 8. Calculated impact of monolayer biofilm location on the water flux, with spacers in the flow channels. (a) Calculated flux along the membrane. (b) Average flux over the whole membranem surface. The four considered scenarios were: no biofilm (continuous blue line), biofilm only on the feed side (blue dotted line), biofilm only at the draw side (grey dash-dot line) and biofilm on both sides (red dashed line) of the membrane. Biofilm presence on the draw side of the membrane leads to higher flux decline than the same amount of biomass was present on the feed side. (For interpretation of the references to colour in this figure legend, the reader is referred to the web version of this article.)

supply the numerical models with realistic parameter values.

3.2.3. Biofilm roughness and membrane surface coverage

In general, an average biofilm thickness is reported in the literature, with no or little information regarding the biofilm distribution along the membrane, due to the difficulty to evaluate the local biofilm thickness under operating conditions. Measurements with dyes coloring the liquid phase in a flow channel (e.g., rhodamine) can give a rough estimate of the average biofilm thickness (Prest et al., 2012; Staal et al., 2011). With other imaging techniques such as optical coherence tomography (OCT) and confocal laser scanning microscopy (CLSM) the local biofilm thickness can be accurately measured but only on small areas (Dreszer et al., 2013; Valladares Linares et al., 2015; West et al., 2015). Therefore, to evaluate the impact of membrane coverage with biofilm on the FO flux, numerical simulations were performed with the same amount of biofilm in the feed channel (i.e., same biovolume or average thickness) but with different membrane coverage (i.e., different biofilm roughness and membrane coverage).

Two biofilm types were evaluated with the numerical model. A continuous, constant thickness biofilm covering the whole membrane surface, and a patchy, irregular biofilm covering only 50 percent of the total membrane area. Fig. 7a shows the flux profile along the membrane without biofilm and with irregular and continuous biofilm layers. Relative to the flux obtained in the clean channel, the continuous biofilm yielded 20 percent flux decrease. In the case of the patchy biofilm, the flux decrease depends on the local biofilm thickness. Maximum flux is obtained on the membrane areas not covered by biomass, whereas the flux strongly declines under the biomass colonies which lead to more concentration polarization. The biofilm enhanced concentration polarization (BECP) was also observed in the RO process, both experimentally and explained by numerical simulations (Chong et al., 2008; Herzberg and Elimelech, 2007; Radu et al., 2012, 2010). The average water flux over the whole membrane area was with 7 percent lower for the continuous foulant layer than for the patchy biofilm (6 L $m^{-2}\cdot h^{-1}$ compared with 6.4 L $m^{-2}\cdot h^{-1}$). This effect has been observed also in ultrafiltration (UF) by Martin et al., 2014. Their study concluded that the fouling layer resistance depends not only on the thickness or volume of the fouling layer, but also on its spatial distribution. Namely, for two spatial distributions with the same mean thickness, it was found that the more heterogeneous distribution will have the higher permeate flux (Martin et al., 2014). Our results confirm that the membrane surface

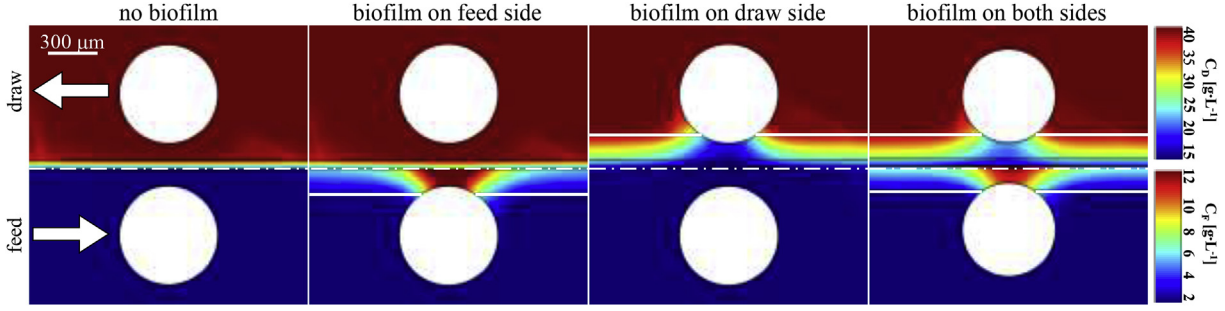

Fig. 9. Calculated salt concentration fields without biofilm and with biofilm on the feed, draw and on both sides of the membrane. The white circles are the spacer fibers in the flow channels, the continuous white line represents the biofilm surface and the white dash-dot line is the membrane active layer. The largest external concentration polarization is induced by the biofilm presence on the draw side of the membrane. Note the different color scales for salt concentration in feed (2–12 kg m^{-3}) and in draw solution (15–40 kg m^{-3}).

coverage by biofilm is indeed an important parameter to be measured and reported, besides the overall biofilm volume or thickness. However, for FO membranes the impact of biofilm resistance is less pronounced than in UF because the membrane resistance in FO is the dominant one, while UF membranes have a lower hydraulic resistance than the biofilm. Typically microfiltration (MF) and UF membranes resistance are between 10^{11} m^{-1} to 10^{13} m^{-1}, while nanofiltration (NF), RO are 10^{-14} m^{-1} to 10^{-15} m^{-1} (Dreszer et al., 2013), compared with the biofilm resistance in this study which was between 10^{-16} and 10^{-17} m^{-1}.

3.2.4. Impact of biofilm location on flux

During indirect water desalination, high salinity water is used as draw solution and impaired-quality water source such as wastewater effluent or urban storm water runoff is used as feed solution (Valladares Linares et al., 2014b). Seawater and brackish water have a high potential as draw solutions in indirect FO processes. In such a case, fouling can occur on both feed and draw sides of the membrane. To evaluate the impact of fouling on the different membrane sides, simulations were run with continuous biofilm layers (i) only on the feed side, (ii) only on the draw side and (iii) on both sides of the membrane.

In general fouling develops faster on the membrane support layer as it was shown by Mi and Elimelech (2008) and Wang et al. (2010). In our study, the membrane support layer is in contact with the draw solution. However, in this model case the biofilm development was not considered: only the impact on membrane performance of the same amount of biomass on the different membrane sides was evaluated (a constant biofilm thickness of 150 μm). A lower water flux resulted when the biofilm was only on the draw side of the membrane, compared with the biofilm on the feed side (6.5 L m^{-2} h^{-1} vs. 5.9 L $m^{-}2$ h^{-1}, respectively) (Fig. 8). This is caused by the higher ECP in the draw channel when a biofilm is present compared with the feed channel (Fig. 9). Since the draw solution has a significantly higher solute concentration compared to the feed solution, the impact of dilutive ECP in the presence of biofilm is higher. As expected, the highest flux decline was obtained when biofilms of 150 μm thickness were present on both sides of the membrane (Fig. 8).

Based on the simulation results it can be concluded that fouling on the draw side of the membrane has a higher impact on the FO process performance than on the feed side. Foulant deposition on the membrane draw side is possible in indirect desalination with FO when seawater or brackish water is used as draw solution (Valladares Linares et al., 2014b). Since the experiments in FO systems mainly focused on fouling accumulation on the membrane feed side (Mi and Elimelech, 2010; Valladares Linares et al., 2014a, 2014b; Wang et al., 2010), experimental studies are needed to further investigate the impact of biofilm formation in the draw side of the FO membrane.

4. Conclusions

The experimental and computational evaluation of biofilm formation in forward osmosis (FO) processes led to the following conclusions:

- Two-dimensional numerical simulations combining fluid flow with salt transport describe well the experimental FO flux measurements at (i) various osmotic pressure differences and (ii) in batch operation with and without biofilm on the membrane active layer.
- The presence of a biofilm on the membrane significantly affects the external concentration polarization and can become the limiting factor for water permeation in FO systems.
- Unlike in RO systems, the same amount of biomass leads to more water flux decline when the biofilm develops on the draw side of the FO membrane compared to the biofilm formed on the feed side, due to higher concentration polarization induced by foulant layer in the draw channel.
- Not only biofilm properties such as hydraulic permeability and mean thickness, but also the biofilm porosity and spatial heterogeneity must be considered when evaluating biofouling effects on the performance of membrane-based separation systems. Since FO biofilms tend to grow thicker, and more porous than in RO, measurements obtained in FO conditions are needed to reveal how the biofilm parameters change in time and to supply the numerical models with realistic parameter values.

Acknowledgements

The research reported in this publication was supported by funding from King Abdullah University of Science and Technology (KAUST). The authors gracefully acknowledge Andrea Radu (Swiss Federal Institute of Technology Zürich) and Maria Jose Mosqueira Santillan (MSc project, King Abdullah University of Science and Technology) for their support in the initial stages of the numerical model development.

References

Achilli, A., Prante, J.L., Hancock, N.T., Maxwell, E.B., Childress, A.E., 2014. Experimental results from RO-PRO: a next generation system for low-energy desalination. Environ. Sci. Technol. 48, 6437–6443. http://dx.doi.org/10.1021/es405556s.

Araújo, P.A., Kruithof, J.C., Van Loosdrecht, M.C.M., Vrouwenvelder, J.S., 2012. The potential of standard and modified feed spacers for biofouling control. J. Memb. Sci. 403–404, 58–70. http://dx.doi.org/10.1016/j.memsci.2012.02.015.

Baker, J., Stephenson, T., Dard, S., Cote, P., 1995. Characterisation of fouling of nanofiltration membranes used to treat surface waters. Environ. Technol. 16, 977–985. http://dx.doi.org/10.1080/09593331608616335.

Boo, C., Elimelech, M., Hong, S., 2013. Fouling control in a forward osmosis process integrating seawater desalination and wastewater reclamation. J. Memb. Sci. 444, 148–156. http://dx.doi.org/10.1016/j.memsci.2013.05.004.

Bucs, S.S., Linares, R.V., Marston, J.O., Radu, A.I., Vrouwenvelder, J.S., Picioreanu, C., 2015. Experimental and numerical characterization of the water flow in spacer-filled channels of spiral-wound membranes. Water Res. 87, 299–310. http://dx.doi.org/10.1016/j.watres.2015.09.036.

Cath, T.Y., Adams, D., Childress, A.E., 2005. Membrane contactor processes for wastewater reclamation in space: II. Combined direct osmosis, osmotic distillation, and membrane distillation for treatment of metabolic wastewater. J. Memb. Sci. 257, 111–119. http://dx.doi.org/10.1016/j.memsci.2004.07.039.

Chong, T.H., Wong, F., Fane, A., 2008. The effect of imposed flux on biofouling in reverse osmosis: role of concentration polarisation and biofilm enhanced osmotic pressure phenomena. J. Memb. Sci. 325, 840–850. http://dx.doi.org/10.1016/j.memsci.2008.09.011.

Crittenden, O.C., Rhodes Trussell, R., Hand, D.W., Howe, K.G., Tchobanoglous, G., 2012. MWH's Water Treatment: Principles and Design, third ed. ed. John Wiley & Sons, Inc. http://dx.doi.org/10.1002/9781118131473.

Dreszer, C., Vrouwenvelder, J.S., Paulitsch-Fuchs, A.H., Zwijnenburg, A., Kruithof, J.C., Flemming, H.C., 2013. Hydraulic resistance of biofilms. J. Memb. Sci. 429, 436–447. http://dx.doi.org/10.1016/j.memsci.2012.11.030.

Gray, G.T., McCutcheon, J.R., Elimelech, M., 2006. Internal concentration polarization in forward osmosis: role of membrane orientation. Desalination 197, 1–8. http://dx.doi.org/10.1016/j.desal.2006.02.003.

Herzberg, M., Elimelech, M., 2007. Biofouling of reverse osmosis membranes: role of biofilm-enhanced osmotic pressure. J. Memb. Sci. 295, 11–20. http://dx.doi.org/10.1016/j.memsci.2007.02.024.

Hickenbottom, K.L., Hancock, N.T., Hutchings, N.R., Appleton, E.W., Beaudry, E.G., Xu, P., Cath, T.Y., 2013. Forward osmosis treatment of drilling mud and fracturing wastewater from oil and gas operations. Desalination 312, 60–66. http://dx.doi.org/10.1016/j.desal.2012.05.037.

Holloway, R.W., Childress, A.E., Dennett, K.E., Cath, T.Y., 2007. Forward osmosis for concentration of anaerobic digester centrate. Water Res. 41, 4005–4014. http://dx.doi.org/10.1016/j.watres.2007.05.054.

Hoover, L.A., Phillip, W.A., Tiraferri, A., Yip, N.Y., Elimelech, M., 2011. Forward with osmosis: emerging applications for greater sustainability. Environ. Sci. Technol. 45, 9824–9830. http://dx.doi.org/10.1021/es202576h.

Kwan, S.E., Bar-Zeev, E., Elimelech, M., 2015. Biofouling in forward osmosis and reverse osmosis: measurements and mechanisms. J. Memb. Sci. 493, 703–708.

http://dx.doi.org/10.1016/j.memsci.2015.07.027.
Lewandowski, Z., 2000. Notes on biofilm porosity. Water Res. 34, 2620–2624. http://dx.doi.org/10.1016/S0043-1354(00)00186-X.
Li, D., Zhang, X., Simon, G.P., Wang, H., 2013. Forward osmosis desalination using polymer hydrogels as a draw agent: influence of draw agent, feed solution and membrane on process performance. Water Res. 47, 209–215. http://dx.doi.org/10.1016/j.watres.2012.09.049.
Li, Z.Y., Yangali-Quintanilla, V., Valladares-Linares, R., Li, Q., Zhan, T., Amy, G., 2012. Flux patterns and membrane fouling propensity during desalination of seawater by forward osmosis. Water Res. 46, 195–204. http://dx.doi.org/10.1016/j.watres.2011.10.051.
Martin, K.J., Bolster, D., Derlon, N., Morgenroth, E., Nerenberg, R., 2014. Effect of fouling layer spatial distribution on permeate flux: a theoretical and experimental study. J. Memb. Sci. 471, 130–137. http://dx.doi.org/10.1016/j.memsci.2014.07.045.
McCutcheon, J.R., Elimelech, M., 2006. Influence of concentrative and dilutive internal concentration polarization on flux behavior in forward osmosis. J. Memb. Sci. 284, 237–247. http://dx.doi.org/10.1016/j.memsci.2006.07.049.
McCutcheon, J.R., McGinnis, R.L., Elimelech, M., 2005. A novel ammonia-carbon dioxide forward (direct) osmosis desalination process. Desalination 174, 1–11. http://dx.doi.org/10.1016/j.desal.2004.11.002.
McDonogh, R., Schaule, G., Flemming, H.-C., 1994. The permeability of biofouling layers on membranes. J. Memb. Sci. 87, 199–217. http://dx.doi.org/10.1016/0376-7388(93)E0149-E.
Mi, B., Elimelech, M., 2010. Organic fouling of forward osmosis membranes: fouling reversibility and cleaning without chemical reagents. J. Memb. Sci. 348, 337–345. http://dx.doi.org/10.1016/j.memsci.2009.11.021.
Mi, B., Elimelech, M., 2008. Chemical and physical aspects of organic fouling of forward osmosis membranes. J. Memb. Sci. 320, 292–302. http://dx.doi.org/10.1016/j.memsci.2008.04.036.
Modern Water Inc, October 2012. Modern water commissions Al Najdah FO plant. Membr. Technol. 2012 (10) http://dx.doi.org/10.1016/S0958-2118(12)70202-1. Pages 4.
Mulder, M., 1996. Basic Principles of Membrane Technology, Second. ed. Springer, Netherlands. http://dx.doi.org/10.1007/978-94-009-1766-8.
Phillip, W.A., Yong, J.S., Elimelech, M., 2010. Reverse draw solute permeation in forward osmosis: modeling and experiments. Environ. Sci. Technol. 44, 5170–5176. http://dx.doi.org/10.1021/es100901n.
Picioreanu, C., Vrouwenvelder, J.S., van Loosdrecht, M.C.M., 2009. Three-dimensional modeling of biofouling and fluid dynamics in feed spacer channels of membrane devices. J. Memb. Sci. 345, 340–354. http://dx.doi.org/10.1016/j.memsci.2009.09.024.
Prest, E.I., Staal, M., Kühl, M., van Loosdrecht, M.C.M., Vrouwenvelder, J.S., 2012. Quantitative measurement and visualization of biofilm O2 consumption rates in membrane filtration systems. J. Memb. Sci. 392–393, 66–75. http://dx.doi.org/10.1016/j.memsci.2011.12.003.
Qin, J.J., Chen, S., Maung, H.O., Kekre, K.A., Cornelissen, E.R., Ruiken, C.J., 2010. Experimental studies and modeling on concentration polarization in forward osmosis. Water Sci. Technol. 61, 2897–2904. http://dx.doi.org/10.2166/wst.2010.078.
Radu, A.I., Vrouwenvelder, J.S., van Loosdrecht, M.C.M., Picioreanu, C., 2012. REMOVED: modeling biofouling, scaling and combined fouling in reverse osmosis membrane devices. Procedia Eng. 44, 341–342. http://dx.doi.org/10.1016/j.proeng.2012.08.409.
Radu, A.I., Vrouwenvelder, J.S., van Loosdrecht, M.C.M., Picioreanu, C., 2010. Modeling the effect of biofilm formation on reverse osmosis performance: flux, feed channel pressure drop and solute passage. J. Memb. Sci. 365, 1–15. http://dx.doi.org/10.1016/j.memsci.2010.07.036.
Sagiv, A., Zhu, A., Christofides, P.D., Cohen, Y., Semiat, R., 2014. Analysis of forward osmosis desalination via two-dimensional FEM model. J. Memb. Sci. 464, 161–172. http://dx.doi.org/10.1016/j.memsci.2014.04.001.
Schock, G., Miquel, A., 1987. Mass transfer and pressure loss in spiral wound modules. Desalination 64, 339–352. http://dx.doi.org/10.1016/0011-9164(87)90107-X.
Shannon, M.A., Bohn, P.W., Elimelech, M., Georgiadis, J.G., Mariñas, B.J., Mayes, A.M., 2008. Science and technology for water purification in the coming decades. Nature 452, 301–310. http://dx.doi.org/10.1038/nature06599.
Staal, M., Prest, E.I., Vrouwenvelder, J.S., Rickelt, L.F., K??hl, M., Kühl, M., 2011. A simple optode based method for imaging O 2 distribution and dynamics in tap water biofilms. Water Res. 45, 5027–5037. http://dx.doi.org/10.1016/j.watres.2011.07.007.
Su, J., Chung, T.-S., 2011. Sublayer structure and reflection coefficient and their effects on concentration polarization and membrane performance in FO processes. J. Memb. Sci. 376, 214–224. http://dx.doi.org/10.1016/j.memsci.2011.04.031.
Subramani, A., Kim, S., Hoek, E., 2006. Pressure, flow, and concentration profiles in open and spacer-filled membrane channels. J. Memb. Sci. 277, 7–17. http://dx.doi.org/10.1016/j.memsci.2005.10.021.
Suh, C., Lee, S., 2013. Modeling reverse draw solute flux in forward osmosis with external concentration polarization in both sides of the draw and feed solution. J. Memb. Sci. 427, 365–374. http://dx.doi.org/10.1016/j.memsci.2012.08.033.
Tan, C.H., Ng, H.Y., 2008. Modeling of external and internal concentration polarization effect on flux behaviour of forward osmosis. Water Sci. Technol. Water Supply 8, 533. http://dx.doi.org/10.2166/ws.2008.116.
Valladares Linares, R., Bucs, S.S., Li, Z., AbuGhdeeb, M., Amy, G., Vrouwenvelder, J.S., 2014a. Impact of spacer thickness on biofouling in forward osmosis. Water Res. 57, 223–233. http://dx.doi.org/10.1016/j.watres.2014.03.046.
Valladares Linares, R., Li, Z., Abu-Ghdaib, M., Wei, C.H., Amy, G., Vrouwenvelder, J.S., 2013. Water harvesting from municipal wastewater via osmotic gradient: an evaluation of process performance. J. Memb. Sci. 447, 50–56. http://dx.doi.org/10.1016/j.memsci.2013.07.018.
Valladares Linares, R., Li, Z., Sarp, S., Bucs, S.S., Amy, G., Vrouwenvelder, J.S., 2014b. Forward osmosis niches in seawater desalination and wastewater reuse. Water Res. 66, 122–139. http://dx.doi.org/10.1016/j.watres.2014.08.021.
Valladares Linares, R., Wexler, A.D., Bucs, S.S., Dreszer, C., Zwijnenburg, A., Flemming, H.-C., Kruithof, J.C., Vrouwenvelder, J.S., 2015. Compaction and relaxation of biofilms. Desalin. Water Treat. 1–13. http://dx.doi.org/10.1080/19443994.2015.1057036.
Vrouwenvelder, J.S., Graf von der Schulenburg, D.A.A., Kruithof, J.C.C., Johns, M.L.L., van Loosdrecht, M.C.M.C.M., 2009. Biofouling of spiral-wound nanofiltration and reverse osmosis membranes: a feed spacer problem. Water Res. 43, 583–594. http://dx.doi.org/10.1016/j.watres.2008.11.019.
Vrouwenvelder, J.S., Manolarakis, S.A., van der Hoek, J.P., van Paassen, J.A.M., van der Meer, W.G.J., van Agtmaal, J.M.C., Prummel, H.D.M., Kruithof, J.C., van Loosdrecht, M.C.M., 2008. Quantitative biofouling diagnosis in full scale nanofiltration and reverse osmosis installations. Water Res. 42, 4856–4868. http://dx.doi.org/10.1016/j.watres.2008.09.002.
Wang, Y., Wicaksana, F., Tang, C.Y., Fane, A.G., 2010. Direct microscopic observation of forward osmosis membrane fouling. Environ. Sci. Technol. 44, 7102–7109. http://dx.doi.org/10.1128/JVI.01705-10.
Werner, C.M., Logan, B.E., Saikaly, P.E., Amy, G.L., 2013. Wastewater treatment, energy recovery and desalination using a forward osmosis membrane in an air-cathode microbial osmotic fuel cell. J. Memb. Sci. 428, 116–122. http://dx.doi.org/10.1016/j.memsci.2012.10.031.
West, S., Wagner, M., Engelke, C., Horn, H., 2015. Optical coherence tomography for the in situ three-dimensional visualization and quantification of feed spacer channel fouling in reverse osmosis membrane modules. J. Memb. Sci. 498, 345–352. http://dx.doi.org/10.1016/j.memsci.2015.09.047.
Xie, M., Lee, J., Nghiem, L.D., Elimelech, M., 2015. Role of pressure in organic fouling in forward osmosis and reverse osmosis. J. Memb. Sci. 493, 748–754. http://dx.doi.org/10.1016/j.memsci.2015.07.033.
Yangali-Quintanilla, V., Li, Z., Valladares, R., Li, Q., Amy, G., 2011. Indirect desalination of Red Sea water with forward osmosis and low pressure reverse osmosis for water reuse. Desalination 280, 160–166. http://dx.doi.org/10.1016/j.desal.2011.06.066.
Yoon, H., Baek, Y., Yu, J., Yoon, J., 2013. Biofouling occurrence process and its control in the forward osmosis. Desalination 325, 30–36. http://dx.doi.org/10.1016/j.desal.2013.06.018.
Zhang, T.C., Bishop, P.L., 1994. Density, porosity, and pore structure of biofilms. Water Res. 28, 2267–2277. http://dx.doi.org/10.1016/0043-1354(94)90042-6.
Zou, S., Wang, Y.N., Wicaksana, F., Aung, T., Wong, P.C.Y., Fane, A.G., Tang, C.Y., 2013. Direct microscopic observation of forward osmosis membrane fouling by microalgae: critical flux and the role of operational conditions. J. Memb. Sci. 436, 174–185. http://dx.doi.org/10.1016/j.memsci.2013.02.030.